PERGAMON

International Journal of Multiphase Flow 25 (1999) 887–919

International Journal of Multiphase Flow

www.elsevier.com/locate/ijmulflow

Numerical study of the oscillations of a non-spherical bubble in an inviscid, incompressible liquid. Part I: free oscillations from non-equilibrium initial conditions

Neil K. McDougald*, L. Gary Leal

University of California, Department of Chemical Engineering, Santa Barbara, CA 93106-5080, USA

Received 24 March 1998; received in revised form 6 November 1998

Abstract

We consider the dynamics of a non-spherical gas bubble undergoing large amplitude oscillations of shape and volume in an inviscid, incompressible fluid. Solutions obtained via either a spectral or boundary-integral technique. The primary objective is to explore the coupling between oscillations of bubble volume and shape, starting from initial conditions where the bubble is either deformed in shape or at a non-equilibrium volume, and the fluid is stationary far from the bubble. For bubbles with a spherical mean shape, we consider conditions that are near 2:1 resonance (as predicted by small amplitude theory). We find that the small deformation theory provides a reasonable estimate of the conditions for shape instability, and of the time scales for resonant interactions between the purely radial and shape modes. However, other features such as the onset of higher order shape modes, or strong departures from Rayleigh–Plesset predictions, are not well approximated by the small amplitude theory. Bubbles which have a non-spherical mean shape exhibit two frequency ranges, corresponding to 2:1 and 1:1 resonance, where Rayleigh–Plesset theory is insufficient to describe the volume response of an oscillating bubble. We also show that purely radial initial conditions can lead to bubble breakup as energy is transferred from purely radial oscillations to shape oscillations.

1. Introduction

Oscillations of bubble volume and shape play an important role in many natural and industrial processes. The most extensively studied phenomenon is the production of sound by

* Corresponding author.

0301-9322/99/$ - see front matter
PII: S0301-9322(98)00073-1

oscillations of bubble volume, based upon the well-known Rayleigh–Plesset analysis of an oscillating *spherical* bubble (Plesset and Prosperetti, 1997; Prosperetti, 1984a, 1984b). Shape oscillations for bubbles of constant volume have also been studied in the context of bubble breakup (Sevik and Park, 1973; Miksis, 1981; Kang and Leal, 1987, 1988, 1989, 1990). Until recently, however, there has been relatively little work on understanding the coupling between oscillations of volume and shape. The primary issue addressed was the parametric instability of oscillating spherical bubbles to infinitesimal perturbations of shape. However, this picture changed dramatically with the suggestion of Longuet-Higgins (1989a) that deformations of shape, as encountered in bubbles entrained by breaking waves in the ocean, might represent a significant source of sound via resonant excitation of *volume* oscillations even for a bubble that was initially at its equilibrium volume. This suggestion, and the work that emanated from it, has renewed interest in the dynamics of non-spherical bubble oscillations.

The vast majority of authors, following Longuet-Higgins (1989a), focused on the changes in oscillations of bubble volume through resonant interactions with one or more shape modes (Longuet-Higgins, 1989b; Ffowcs Williams and Guo, 1991; Mei and Zhow, 1991; Yang et al., 1993; Feng and Leal, 1993, 1994). These studies considered only small amplitude oscillations of volume and shape using the method of domain perturbations and various techniques from the analysis of non-linear oscillators to resolve the fast timescale associated with the natural frequency of volume and/or shape oscillations, and the slow timescale characterizing the resonant exchange of energy between the volume and shape modes. This, and related work is summarized in the recent review by Feng and Leal (1997). In general, for an inviscid fluid, the interaction between modes leads to a *continuous exchange* of energy between oscillations of volume and shape, yielding the possibility of significant shape change resulting from an initial perturbation of the volume, as well as radial oscillations from an initial perturbation of shape.

Interactions between radial and shape oscillations have been found in the small deformation theory to occur under conditions where the natural frequency of the purely radial mode is equal or nearly equal to an integer multiple of the natural frequency for one of the Legendre modes that describe the bubble shape. Longuet-Higgins (1989a,b) considered 2:1 resonance in which the natural frequency of the radial oscillation is twice that of the shape mode, and the interaction is via quadratic resonance. For bubbles with a spherical steady-state shape, the most significant interactions between changes in volume and shape are these quadratic, 2:1 resonance interactions. However, resonant interactions are also predicted for radial mode frequencies equal to larger integer multiples of the shape mode frequency.

When the steady-state shape of a bubble is *not* spherical due, for example, to an external flow or an anisotropic pressure field, the interaction between changes in volume and shape can be enhanced. In addition to the 2:1 and higher resonances, Yang et al. (1993) and Feng and Leal (1993) have shown in this case that energy is exchanged when the natural frequency for radial oscillations *equals* the frequency of one of the shape modes, i.e. $\omega_0 \approx \omega_n$. We refer to this as 1:1 resonance. It is a consequence of the fact that as the bubble volume increases, the magnitude of changes in the interface pressure or stress, which cause the mean shape deformation, are enhanced.

In this paper, numerical simulations are used to extend our current understanding of these phenomena, by considering larger amplitude volume and shape oscillations. In the small amplitude limit, the amount of time required for a significant exchange of energy via resonant

interactions is very long, of $O(\epsilon^{-1})$ where ϵ is the magnitude of shape or volume perturbations. It is thus likely that such small amplitude resonant effects would be damped by viscous effects before playing a prominent role in the dynamics of a real bubble. At finite amplitude, however, the timescale for interaction between modes will decrease and we may expect the small amplitude resonance analysis to provide qualitative insight into the bubble behavior. In addition, such interactions will occur even for conditions where the natural frequencies are not near resonance. Finally, although the theoretical, small amplitude theory also predicts that the interactions occur only between radial oscillations and a *single* Legendre shape mode, it is expected that more complicated shape oscillations will be excited at finite amplitude, due to mode coupling between the various shape modes. From a practical point of view, it is important to establish when this occurs, because it represents a limit on the regime where we might expect the small amplitude theory to provide a useful, low-dimensional, alternative to the Rayleigh–Plesset theory. The use of a numerical method to simulate the bubble response in the finite deformation regime will test these hypotheses and provide additional insight into the physics underlying the dynamics of bubble oscillations.

2. Background

In order to understand the physics underlying the numerical results presented here, it is essential to give some details of the small amplitude analytical treatment of an oscillating non-spherical bubble. The following summary is based upon the work by Feng and Leal (1993) and we adopt their notation.

Let the small amplitude limit, the dynamics of bubble oscillations is largely determined by the proximity to resonance conditions. If the natural frequency for volume oscillations in dimensional form is denoted as $\hat{\omega}_0$,

$$\hat{\omega}_0^2 \equiv \frac{\Gamma}{a^3\rho}\left[3\gamma\left(\frac{P_\infty}{\Gamma/a}+2\right)-2\right] \tag{1}$$

and the natural frequency of the nth shape mode (described by the Legendre polynomial P_n) as $\hat{\omega}_n$,

$$\hat{\omega}_n^2 \equiv \frac{\Gamma}{a^3\rho}(n-1)(n+1)(n+2) \tag{2}$$

then exact resonance occurs when $\hat{\omega}_0 - k\hat{\omega}_n = 0$ for integer k.[1] Hereafter, $\hat{\omega}_0$ and $\hat{\omega}_n$ will be replaced by their dimensionless equivalents ω_0 and ω_n, which have been nondimensionalized by $(\Gamma/(a^3\rho))^{1/2}$.

In the small amplitude theories, it is assumed that any differences from exact resonance conditions is small, $O(\epsilon)$, and this is quantified by a 'detuning' parameter, β_0, defined such that

[1] Here, Γ is the interfacial tension, a is the undeformed radius, ρ the liquid density, P_∞ the ambient pressure and γ is the ratio of specific heats (C_p/C_v).

$$\omega_0 - k\omega_n = \epsilon\beta_0 \tag{3}$$

where ϵ denotes the characteristic amplitude of the shape and volume perturbations. For convenience, in what follows, we will use β_0 for $k=2$ (2:1 resonance), and β_0^* for $k=1$ (1:1 resonance). When the detuning is large ($\omega_0 - k\omega_n > O(\epsilon)$) there is no interaction between modes according to the small amplitude, theoretical predictions. For small detuning ($\omega_0 - k\omega_n \leqslant O(\epsilon)$), however, the nth shape mode and the radial mode are in a near resonant (or exact resonant) state, and energy exchange between these oscillating modes can be significant, on a timescale of $O(\epsilon^{-1})$ relative to the natural timescale for radial or shape oscillations, $O(2\pi/\omega_0)$ or $O(2\pi/\omega_n)$.

The detuning parameters, β_0 and β_0^*, are appropriate for bubbles with a mean *spherical* shape. However, the small amplitude theory and our present study also consider bubbles that have a non-spherical steady-state shape. While there are many mechanisms by which a bubble may achieve a deformed steady-state shape, we consider the simplest case of a non-spherical mean shape due to a non-uniform pressure distribution on the bubble interface, $A(\eta, t) = A_0 + A_n P_n(\eta)$, which might be envisioned as a 'radiation' pressure produced via modulated ultrasonic wave fields in an experimental levitation system (Marston, 1980). The presence of a mean deformation causes the natural frequencies for volume and shape oscillations to shift relative to their values for *spherical* bubbles. Therefore, when the mean shape of a bubble is non-spherical, the detuning parameters based upon the natural frequencies for a spherical bubble, β_0 and β_0^*, must be modified to account for these changes. The small amplitude theory introduces *effective* detuning parameters, β and β^* that incorporate the shifts in natural frequencies, to quantify the proximity to exact resonance conditions in these cases:

$$\beta = \beta_0 + \left(\frac{3\gamma - 1}{4\omega_n} + \frac{3\gamma - 1}{8\omega_n^3}\right)A_0 - \frac{(n+1)(2n+1)k_n}{(3n+1)\omega_n}\left(\frac{4(n+1)}{\omega_n^2} + \frac{10 - n}{2}\right)A_n \tag{4}$$

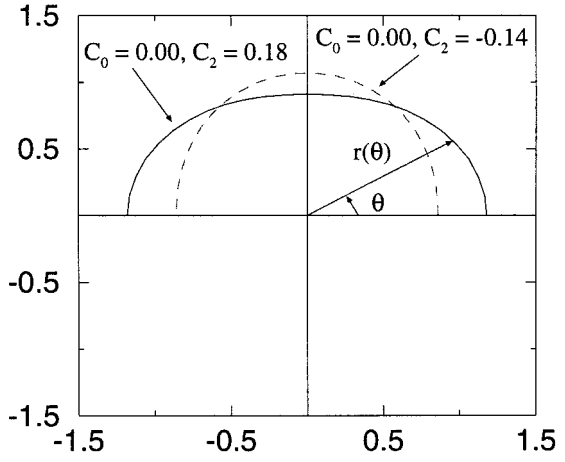

Fig. 1. The position of the interface given by the function $r(\theta)$.

$$\beta^* = \beta_0^* + \left(\frac{3\gamma - 1}{2\omega_n} + \frac{3\gamma - 1}{\omega_n^3}\right)A_0 - \frac{(n+1)(2n+1)k_n}{(3n+1)\omega_n}\left(\frac{2(n+1)}{\omega_n^2} + \frac{10-n}{4}\right)A_n \tag{5}$$

$$k_n = \left(\frac{(n-1)!!}{(n/2)!}\right)^3 \frac{(3n/2)!}{(3n-1)!!} \quad n \text{ even}$$

$$k_n = 0 \quad n \text{ odd}$$

for 2:1 and 1:1 resonance, respectively.

For presentation of the present work, as well as comparisons with the small deformation theories, it is convenient to introduce a common notation to describe the changes in bubble volume and shape. The concept of radial and shape *modes* and their associated amplitudes is particularly important here as the numerical results are most simply represented in terms of the amplitudes of the modes as functions of time. For simplicity, we consider only axisymmetric deformations of shape, but the fact that the azimuthal modes are degenerate in the small deformation limit suggests that the results are actually quite general. The central idea, illustrated in Fig. 1, is that the interface of a bubble at any time can be described by a function $r(\theta)$ which can be approximated by a summation of Legendre polynomials:

$$r(\theta) = 1 + f(\theta) \approx 1 + \sum_{j=0}^{\infty} C_j P_j(\cos\theta) \tag{6}$$

where the coefficients, C_j, are given by

$$C_j = \frac{2j+1}{2}\int_0^{\pi} f(\theta) P_j(\cos\theta)\ \sin\theta\ \mathrm{d}\theta \tag{7}$$

The above equations (6) and (7) are general and *do not* assume that the deviation from spherical geometry is infinitesimal. The ability to describe shapes by Legendre modes permits the finite amplitude numerical results to be compared directly with small amplitude predictions. This is a generalized Fourier representation of a function and is useful in the analytical problem because the solution to Laplace's equation in spherical coordinates requires Legendre polynomials.

In the small amplitude theory, the coefficients of the Legendre modes are $O(\epsilon)$ or smaller, and functions of time that are determined as part of the solution. Utilizing the notation of the small amplitude theory, these amplitude coefficients, C_j, can be explicitly expressed in the form

$$C_j = \epsilon C_j^{(1)} + \epsilon^2 C_j^{(2)} + O(\epsilon^3) + \text{c.c.} \tag{8}$$

where

$$C_j^{(1)} = \frac{1}{2}\alpha_{1,j}(\tau)\ \mathrm{e}^{i\delta_j t} \quad \text{with} \quad \delta_j = k\omega_n \quad j = 0$$

$$C_j^{(1)} = \frac{1}{2}\alpha_{1,j}(\tau)\ \mathrm{e}^{i\delta_j t} \quad \text{with} \quad \delta_j = \omega_n \quad j = n \tag{9}$$

and

$$C_j^{(2)} = \sum_{m=0}^{2k} \alpha_{2,m,j}(\tau)\ \mathrm{e}^{im\omega_n t} \tag{10}$$

In the small amplitude theory $\alpha_{1,j}=0$ for all $j\neq 0$ or n where n corresponds to the shape mode that is resonant (or near-resonant) with the radial mode with $\omega_0 = k\omega_n$ *fixed* and $\tau=\epsilon t$. The two nonzero amplitude functions at $O(\epsilon)$ are governed by a coupled pair of nonlinear ordinary differential equations arising from the solvability conditions from the small deformation analysis. The details of the dynamics depend upon the value of k in Eq. (3). A detailed summary of the results for $k=1$, 2 can be found in the recent review by Feng and Leal (1997). Here, we briefly recapitulate the main results.

For the case when $k=2$, the interaction between the P_0 and P_n modes exhibits *quadratic* resonance as indicated earlier, and this occurs whether the steady-state shape is spherical or non-spherical. In general, at $O(\epsilon)$, there is a continuous exchange of energy back and forth between these two modes, with conservation of total energy in the inviscid limit. For all conditions, however, the purely radial oscillation, i.e. $\alpha_{1,0}=a$ nonzero constant and $\alpha_{1,n}=0$, is a fixed point solution of the coupled amplitude equations. The stability of this solution, and the qualitative nature of the coupling between modes depends upon the magnitude of the *effective* detuning parameter defined in Eq. (4), relative to a critical value

$$|\ \epsilon\beta\ |_{\mathrm{cr}} = 2\epsilon r = \frac{(4n-1)\omega_n}{4}\left[\epsilon\ |\ \alpha_{1,0}\ | + \frac{\epsilon\ |\ \alpha_{1,n}\ |}{2\sqrt{(n+1))(2n+1)}}\right] \tag{11}$$

which depends on the amplitudes of the P_0 and P_n modes, according to the right-hand side of Eq. (11). It may be noted that this term is constant, independent of time, for an inviscid fluid. Eq. (11) has been multiplied by ϵ because the level of detuning $\epsilon\beta$ will be the significant quantity for the numerical results presented later. For $\beta > \beta_{\mathrm{cr}}$, there is relatively little interaction between the radial and shape modes (P_0 and P_n), and the purely radial oscillation is stable in the sense that infinitesimal perturbations of shape remain infinitesimal for all time in the inviscid limit. In this case, there is also a second fixed point solution that corresponds to a dominant shape mode oscillation with only weak coupling to radial motion. For $\beta < \beta_{\mathrm{cr}}$, one the other hand, the nature of the solution for $\alpha_{1,0}$ and $\alpha_{1,n}$ changes. The purely radial fixed point solution bifurcates into an elliptic and hyperbolic pair. The hyperbolic point remains at the purely radial point in the solution domain, but it is *unstable* in the sense that there is a homoclinic branch of solutions that emanates from it, so that infinitesimal perturbations of shape now lead to finite amplitudes in the shape mode. Indeed, as $\beta \to 0$, the solution branch that emanates from the purely radial position in the solution domain passes through the point corresponding to a pure shape oscillation, meaning that there will be a complete transfer of energy from radial oscillations to shape oscillations before the system eventually reverts back again to radial oscillations. The critical bifurcation point β_{cr} corresponds to the onset of parametric instability to infinitesimal perturbations of shape.

The case of 1:1 resonance, corresponding to $\omega_0 - \omega_n = O(\epsilon)$, is fundamentally different. First, it only appears when there is a mean deformation of shape. Second, though the strength of interactions between the P_0 and P_n mode increases as the effective detuning parameter β^*, defined by Eq. (5), becomes smaller, there is no critical value. The nature of the solutions and the strength of interactions changes smoothly and monotonically as the value of β^* changes. Finally, although there are still two fixed points in the solution domain for 1:1 resonance, where the amplitude functions $\alpha_{1,0}$ and $\alpha_{1,n}$ are time *independent*, neither of these is coincident with pure radial or pure shape oscillations. A small perturbation of shape from spherical will always lead to a shape oscillation of finite amplitude (the magnitude depending upon the degree of detuning, i.e. on the magnitude of β^*).

The analysis summarized above leads to the conclusion that there will generally be interactions between purely radial oscillations, the oscillations of bubble shape, the strength of which depends upon proximity to a resonant condition where $\omega_0 - k\omega_n = O(\epsilon)$. When this occurs, there is an exchange of energy between the purely radial and shape modes, which implies that the magnitude of radial oscillations will generally be smaller than what would be predicted by the Rayleigh–Plesset theory. When the small amplitude approximation can be applied, the coupled pair of equations for the amplitude functions, $\alpha_{1,0}$ and $\alpha_{1,n}$, might then provide an alternative to Rayleigh–Plesset theory as a means to predict, for example, the acoustic signature of a bubble. Of course, the small amplitude theory is restricted, in principle, to *infinitesimal* perturbations of volume or shape from a steady-state condition, and leads to coupling between radial oscillations and a single shape mode. As is often the case with perturbation theories, one may hope that the small amplitude theory would be at least qualitatively representative of the bubble behavior for non-infinitesimal perturbations. To test the range of applicability of the small amplitude theory and increase our understanding of the dynamics of non-spherical bubbles, it is necessary to consider deformations of shape and volume that are not small. For this purpose, we turn to numerical simulations, as described in the remainder of this paper, which is the first of a pair. In this first paper, we consider free oscillations in an inviscid fluid, starting from non-equilibrium initial conditions. In the second paper, we consider the bubble response to time-dependent changes in the ambient pressure.

3. Numerical methods

We have utilized two distinct numerical techniques for the solution of flow problems involving finite amplitude oscillations of volume and shape for a single bubble in an unbounded, incompressible liquid. These are: (1) a spectral code which utilizes a modal decomposition of the bubble shape in terms of spherical harmonics, and is suitable for purely inviscid flows; and (2) a boundary-integral technique which is numerically exact for bubbles of arbitrary shape in a fluid whose motion can be described by a potential function, but which can also be applied approximately to systems with weak viscosity.

3.1. The spectral method

We employ a traditional spectral method as discussed in Fletcher (1991) that is based on the

preceding analytical work for small amplitude oscillations (Yang et al., 1993; Feng and Leal, 1993, 1994). the method assumes that the bubble surface can be decomposed into a finite series of Legendre polynomials with time-dependent coefficients, and that the potential function can likewise be represented by a series of 'decaying' axisymmetric spherical harmonics based on Legendre polynomials. Thus, we automatically satisfy the governing equation for potential flow throughout the domain and are left with the time-dependent coefficients of the shape and potential functions to satisfy the boundary conditions. As with other spectral methods, we make use of the orthogonality of Legendre polynomials and various recursion relations to generate ordinary differential equations for the time-dependent coefficients. The result of this technique is a system of $2N$ ordinary differential equations where N is the total number of modes kept in the Legendre series. These equations are advanced in time using a fourth-order Runge–Kutta routine to give the evolution of the bubble shape and the external potential. The algorithm is very efficient computationally for small amplitude deformation, but as the number of Legendre modes which must be retained for an accurate solution increases, the computation time increases in proportion to N^2. The convergence of the method with increasing number of retained modes and other details of implementation are reported in McDougald's Ph.D. thesis (1997).

3.2. The boundary integral method

The boundary integral method is well suited to the solution of free surface problems because it does not require the discretization of the computational domain. Instead the solution of the problem is expressed in terms of a distribution of fundamental singularities at the boundaries, and the problem is reduced to solving integral equations, derived from the general solution by application of interface boundary conditions, for the strength of these singularities as a function of position on the interface. The dimension of the problem is thereby reduced by one. Furthermore, the velocity of points on the boundary is obtained directly from the singularity strengths, and it is thus possible to determine the evolution of the interface in time without having to explicitly evaluate the velocity field elsewhere in the domain. In our treatment, we consider only axisymmetric shapes so our domain is two-dimensional and the boundary is represented by a one-dimensional curve.

The main limitation of the boundary integral approach for applications at high Reynolds number is that it requires the velocity field to be expressible in terms of a potential, thereby preventing the explicit inclusion of viscous effects. It is possible, however, to include weak viscous effects if the vorticity is confined to a thin region near the interface (Lundgren and Mansour, 1988). Our implementation of the boundary integral scheme follows Brebbia (1978) which treats the method as a special case of the weighted residual method. The weighting functions are chosen to satisfy Laplace's equation and in fact are fundamental solutions corresponding to point sources on the boundary. The nature of the singularity occurring at each node is therefore known, allowing it to be integrated either analytically, if the boundary is discretized using linear elements, or by an appropriate numerical method for more complicated segmentation of the interface. In our case we use a 32-point Gaussian scheme to evaluate the nodal integrals and a five-point Gaussian scheme for other points along the interface as our elements are determined by a cubic spline interpolation between the nodes. The time

advancement in the code is done using a fourth-order Runge–Kutta routine to update the position and the value of the potential for each node along the boundary. The ability to reproduce the results of Rayleigh–Plesset theory and the convergence of the method with decreasing time-step size and increasing spatial resolution, i.e. number of nodes, are again reported in McDougald (1997).

4. Numerical results

In this first paper, we consider free oscillation of a bubble in a quiescent fluid, with either a spherical or non-spherical mean shape (e.g. due to the effect of an anisotropic radiation pressure for a bubble in an ultrasonic sound field).

4.1. Free oscillations of a bubble with a spherical mean shape

For a spherical bubble in a quiescent fluid, we have noted previously, that the dominant *resonant* interaction is 2:1 resonance between a purely radial oscillation and the shape mode, $P_n(\eta)$, for which $\omega_0 \approx 2\omega_n$. In this instance the detuning parameters β_0 and β are equivalent and the fundamental change in the dynamics of the bubble oscillation is predicted by the small deformation theory to occur at a critical degree of detuning, $|\epsilon\beta|_{cr}$ given by Eq. (11). Hereafter, we refer to the level of detuning $\epsilon\beta = \omega_0 - k\omega_n$ as the detuning parameter because the difference in natural frequencies has direct physical significance. In this section, we consider a series of finite amplitude solutions, with initial perturbations of the radius and P_2 mode of shape deformation, as shown in Table 1, which correspond to three different values of the critical detuning parameter, $|\epsilon\beta|_{cr}$. These values are also listed in Table 1. For each of the cases A–C, we present numerical solutions for a series of different values of the detuning parameter, $\epsilon\beta$, including values both larger and smaller than the 'critical' value, estimated from the small deformation theory. It should be emphasized, of course, that the amplitudes of the shape and volume changes considered here are not small, and hence there is no reason to suppose that the small amplitude results should apply.

The first case, case A, is intended to have small enough initial displacements to be at least close to the regime of validity of the small amplitude theory. Calculations were performed for $\epsilon\beta = 0.000$, -0.010, -0.100, -1.000, and -4.000 as well as for several values near the expected critical value of $|\epsilon\beta|_{cr} = 0.063$. Typical results for a case with strong interactions, $\epsilon\beta = 0.000$, and a case for $|\epsilon\beta| > |\epsilon\beta|_{cr}$, namely -0.100, are shown in Figs 2. and 3 along with the magnitudes of

Table 1
The initial radial and shape disturbances and the predicted critical value of the detuning parameter

Case	$\epsilon\alpha_{1,0}$	$\epsilon\alpha_{1,2}$	$\lvert\epsilon\beta\rvert_{cr}$
A	−0.005	0.010	0.063
B	−0.05	0.10	0.63
C	0.10	0.10	1.22

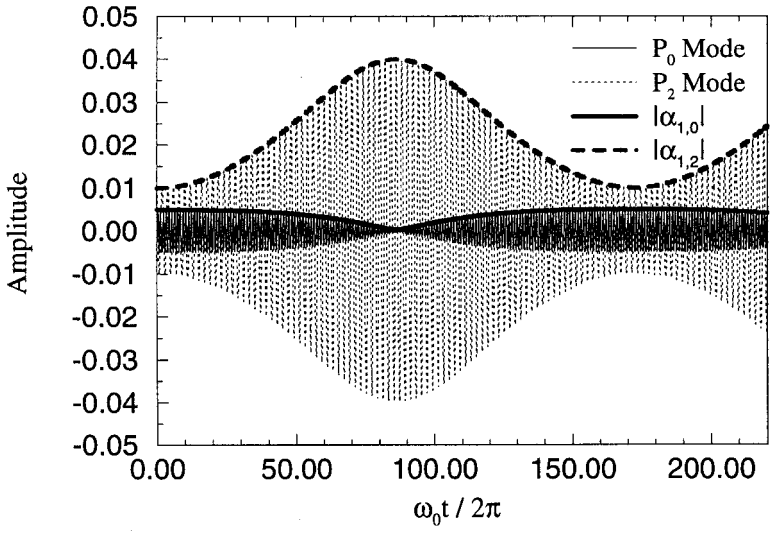

Fig. 2. Amplitudes of the P_0 and P_2 modes and the magnitude of the amplitude functions $\epsilon\alpha_{1,0}(\tau)$ and $\epsilon\alpha_{1,2}(\tau)$ from small deformation theory for Case A (Table 1) with $\epsilon\beta = 0.000$.

$\epsilon\alpha_{1,0}(\tau)$ and $\epsilon\alpha_{1,2}(\tau)$ from the small deformation theory for comparison. These figures, and most of those that follow, show the amplitudes of the oscillating modes as a function of time, non-dimensionalized by $t_c = 2\pi/\hat{\omega}_0$, and are obtained either directly from the spectral computation or by performing a Legendre decomposition of the bubble interface computed using the boundary integral method.

The result in Fig. 2 is a spectral code computation with 10 modes retained for a bubble at the exact resonance condition, $\omega_0 = 2\omega_2$. The initial conditions, in this case represent a small shape deformation, and it can be seen that the purely radial mode is unstable, as there is a nearly complete transfer of energy to the oscillating shape mode which occurs near $\hat{\omega}_0 t/2\pi = 85$. The very long period for change in the amplitudes of the modes is due to the fact that the deformation amplitudes are small, and that the solution trajectory is very close to the homoclinic orbit that emanates from the point in the solution domain corresponding to purely radial oscillations. The fact that small changes in the amplitude of radial oscillations will drive *larger* amplitude shape oscillations is also clearly apparent in Fig. 2. The small amplitude study predicts that a complete transfer of energy from radial to shape modes can yield a maximum change $\Delta_n = 2\sqrt{((n+1)(2n+1))}\Delta_0$ to the amplitude of shape oscillations, given a maximum amplitude Δ_0 of the P_0 mode. This amplification is due to the fact that significantly more work is required to change the bubble volume than to change the bubble shape. As the volume changes, the gas within the bubble must be compressed or expanded, while changes in shape mainly contribute to the energy of the interface due to surface tension. In the present case, with an initial amplitude corresponding to $\Delta_0 = 0.005$ and $\Delta_n = 0.01$ and $n = 2$, the predicted *maximum* amplitude for shape oscillations is 0.048, while the maximum achieved in Fig. 2 is approximately 0.04. The difference is primarily because the initial condition does not fall precisely on the solution trajectory where there is 100% exchange of energy between modes. It

will be noted that the amplitude envelope from the numerical solution agrees very well with predictions of the amplitude functions, $\alpha_{1,0}$ and $\alpha_{1,n}$ from the small deformation theory.

Fig. 3 starts from the same initial conditions, case A, except the amount of detuning has increased to $\epsilon\beta = -0.100$ and thus exceeds the critical value predicted by the small amplitude theory, $|\epsilon\beta|_{cr} = 0.063$. Not surprisingly, there is little exchange of energy between modes and the period of the slow variation in the amplitudes is decreased by approximately a factor of 2. One interesting feature of this result, and all the results for case A with $|\epsilon\beta| \geqslant 0.060$, is that the amplitude of the shape mode never becomes larger than its initial value. This is clear evidence that the volume oscillations are stable under these conditions in agreement with the small deformation theory. The transition to *stable* spherical oscillations, which is found numerically to occur at $|\epsilon\beta|_{cr} = 0.060$, is *conservatively* predicted by the stability limit from small amplitude theory, $|\epsilon\beta|_{cr} = 0.063$. The small difference is presumably due to the fact that even case A is not quite within the small amplitude theory even though the bubble response is still reasonably well predicted by the small amplitude theory.

These long time results were generated using the spectral code because of its efficiency in simulating cases involving only a few modes. The results for the initial conditions of case A exhibited oscillations of the P_0, P_2 and P_4 modes only, for all values of $\epsilon\beta$. The P_4 mode reached a maximum amplitude of 0.0005 for the case of $\epsilon\beta = 0.000$ when the radial oscillations were at their smallest amplitude. Higher order modes had amplitudes less than 10^{-4}. The boundary integral method was used to simulate these cases as well, for a shorter time interval, and the amplitude and volume results agreed with the spectral results over the range tested.

The second case, corresponding to case B in Table 1, has initial perturbation amplitudes increased by a factor of 10, which also increases the predicted critical value, $|\epsilon\beta|_{cr}$, from the small amplitude analysis by a factor of 10. Since the disturbance amplitudes are no longer

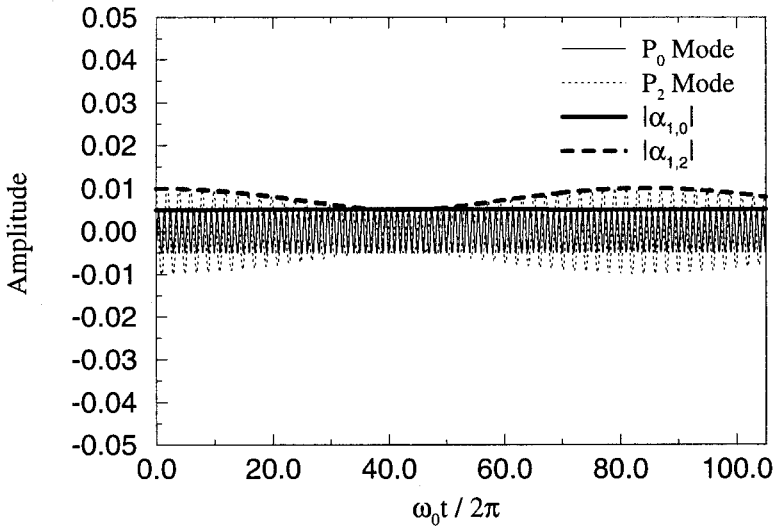

Fig. 3. Amplitudes of the P_0 and P_2 modes and the magnitude of the amplitude functions $\epsilon\alpha_{1,0}(\tau)$ and $\epsilon\alpha_{1,2}(\tau)$ from small deformation theory for Case A (Table 1) with $\epsilon\beta = -0.100$.

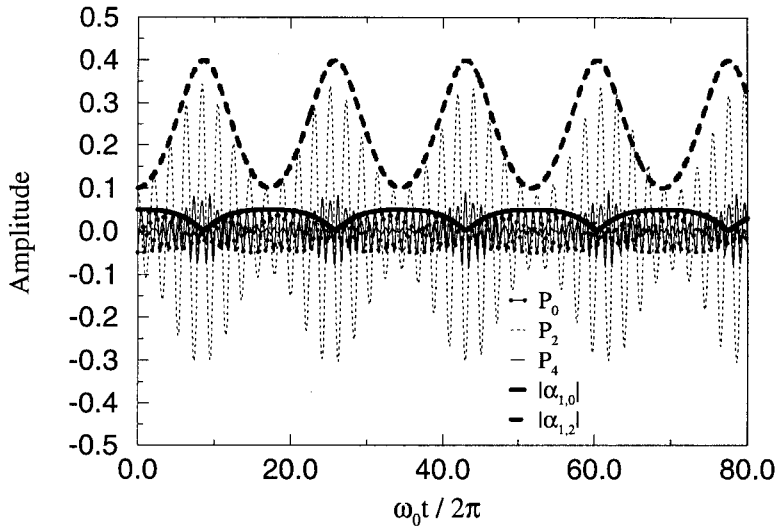

Fig. 4. Amplitudes of the P_0, P_2 and P_4 modes for Case B (Table 1) with $\epsilon\beta = 0.00$.

infinitesimal, we expect to see some difference between the actual magnitude of the detuning parameter where the stability changes, and the predicted value from small amplitude analysis. In addition, we should anticipate that modes other than P_0 and P_2 may be excited. Numerical simulations using both the spectral and boundary integral methods have been done for values of the detuning parameter ranging from $\epsilon\beta = 0.00$ to -4.00 with several cases near the predicted stability boundary, $|\epsilon\beta|_{cr} = 0.63$. Results from the spectral code, retaining a total of 14 shape modes, are shown for representative cases, $\epsilon\beta = 0.00$, -0.40 and -0.60 in Figs. 4–7. The evolution of the bubble interface for $\epsilon\beta = 0.000$ is shown in Fig. 5 which contains several 'snapshots' of the bubble shape as the amplitude of the P_2 mode grows.

For the exact resonance condition of $\epsilon\beta = 0.00$, shown in Fig. 4, there is a strong continuous

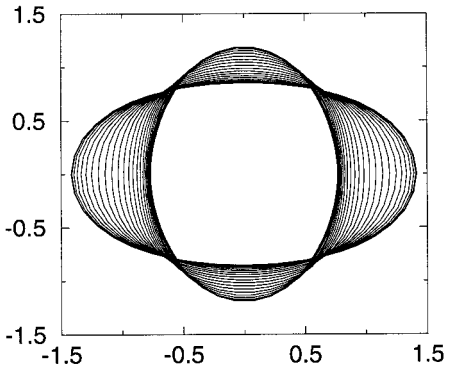

Fig. 5. The evolution of the bubble shapes and the P_2 mode grows for Case B (Table 1 with $\epsilon\beta = 0.00$, $\omega_0 t/2\pi = 7.3 \rightarrow 8.4$.

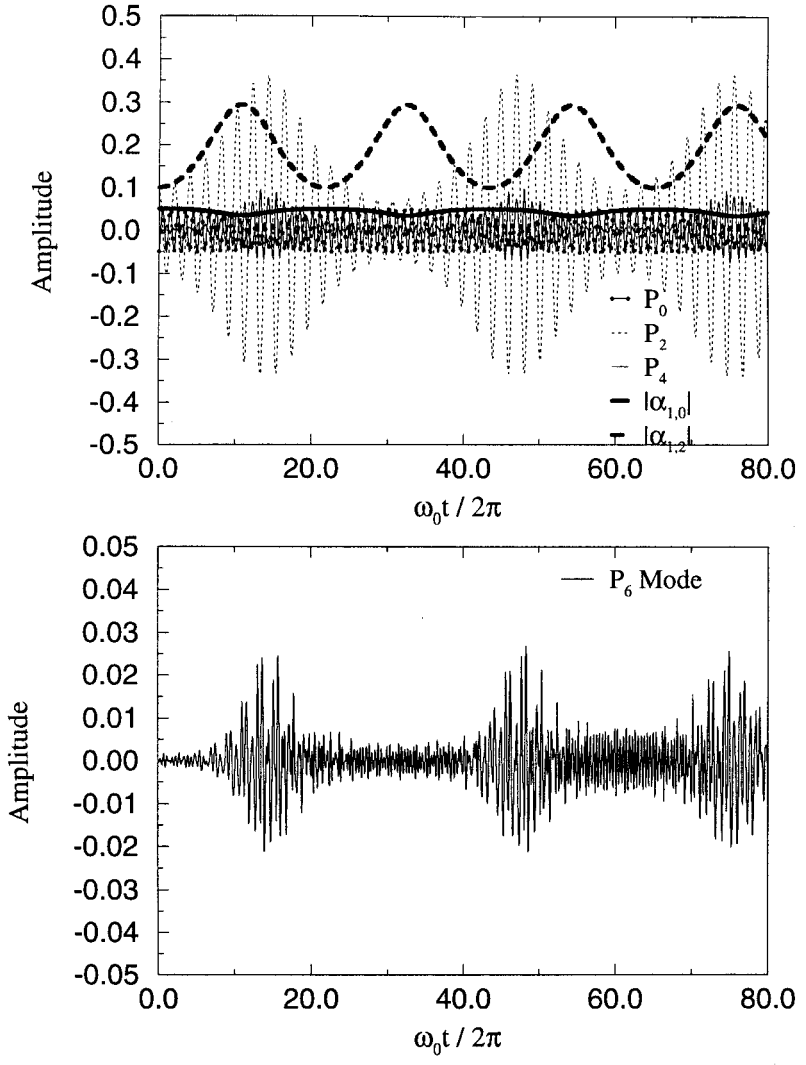

Fig. 6. Amplitudes of the P_0, P_2 and P_4 modes (top) and the P_6 mode (bottom) for Case B (Table 1) with $\epsilon\beta = -0.40$.

exchange of energy between radial and shape oscillations as anticipated above. The period of the slow variation in the amplitudes has shortened to $T \approx 17$ which is approximately a factor of 10 decrease from case A. Surprisingly, in view of the finite amplitude of shape and volume perturbations, this decrease in T is in agreement with the expected scaling of the timescale from the small amplitude theory, $\tau = \epsilon t$. As in the case A the energy transfer is never complete: the maximum amplitude of the P_2 mode oscillation ($\sim$0.35) is less than both the small amplitude prediction of 0.48 and the value of 0.40 that could be expected via a linear scaling from case A as can be seen by comparing the predictions from small deformation theory with the numerical results in Fig. 4. This suggests the onset of a significant degree of nonlinear behavior that is

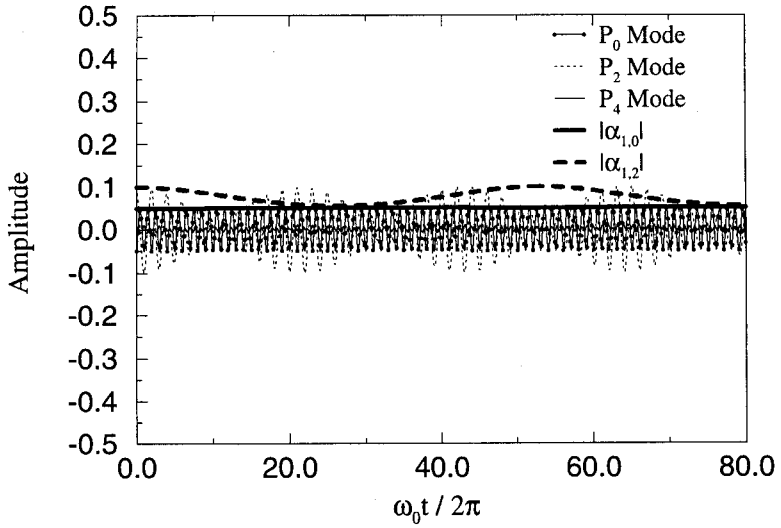

Fig. 7. Amplitudes of the P_0, P_2 and P_4 modes for Case B (Table 1) with $\epsilon\beta = -0.60$.

not accounted for in the small amplitude theory. This is further evidenced by the intermittent appearance of higher, P_4 mode oscillations in Fig. 4. The P_6 and P_8 modes also appear with small amplitude in the simulation, but are not shown in the figure. All of the simulations up to $\epsilon\beta = -0.30$ are qualitatively similar to that shown in Fig. 4, with some modest change in the maximum P_2 amplitude and the period of amplitude modulation. Details can be found in the Ph.D. thesis of McDougald (1997).

The finite amplitude of the P_2 mode has a significant influence on the excitation of higher modes. In Fig. 6, for which $\epsilon\beta = -0.40$, the presence of higher mode oscillations produces a nonlinear change in the bubble dynamics. The period of the slow variation in the amplitudes decreases from $T \approx 30$ to $T \approx 25$ as $\omega_0 t/2\pi$ increases, and there is a gradual decrease in the energy returned to the radial oscillations. This is evidenced by the increase in the *minimum* amplitude of the P_2 mode at $\omega_0 t/2\pi = 60$, versus its value at 30, as well as the gradual increase in the energy of the higher modes, P_4 and P_6. In looking at the P_6 mode only, Fig. 6, the increase in minimum amplitude with time is clearly shown. Although the effect on P_0 is quite small in this specific case, the 'permanent' transfer of energy from radial oscillations to higher order shape modes is characteristic of the finite amplitude problem. These phenomena are already beyond the scope of the small amplitude theory which only accounts for interactions between two modes of appreciable amplitude. They further support the likely importance of nonlinear damping suggested by Longuet-Higgins (1992) wherein the energy available to drive oscillations is decreased as it is transferred to higher mode shape oscillations, where it can be removed more efficiently by viscous dissipation due to the smaller length scales that are generated. It is also interesting to notice that some time was required before the nonlinear features appeared in the P_0 and P_2 modes; seemingly the higher modes must become activated before they can accept enough energy from the lower modes to effect the dynamics of the bubble.

Fig. 7 illustrates the transition to stable radial oscillations as in case A. The small amplitude theory predicts the correct trends in the period of time-modulation of the oscillations of volume and shape increases as you move away from the exact resonance condition, but the period of the slow variation of the amplitude only agrees with the numerical results for small values of $\epsilon\beta$. However, the amplitude of the radial and P_2 mode oscillations is fairly well predicted by the small deformation theory even though the oscillation amplitudes are not infinitesimal. It is, therefore, somewhat surprising that the transition to stable radial oscillations occurs very near the predicted value of $|\epsilon\beta|_{cr}=0.63$ even though the bubble

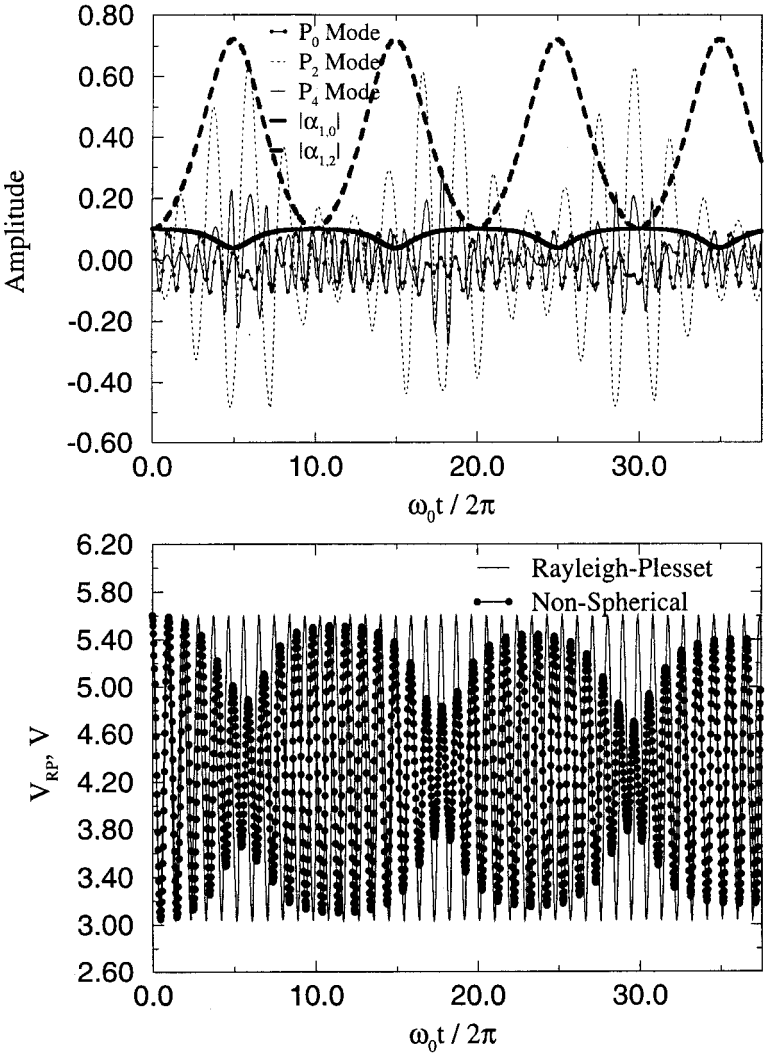

Fig. 8. Amplitudes of the P_0, P_2 and P_4 modes (top) and the volume response V compared with the Rayleigh–Plesset theory V_{RP} (bottom) for Case C (Table 1) with $\epsilon\beta=-0.50$.

response for smaller $|\epsilon\beta|$ already exhibited significantly nonlinear behavior that is beyond the scope of the small deformation theory. The numerical results suggest that finite amplitude, spherical bubble oscillations are slightly more stable than predicted by small amplitude theory.

The final case of Table 1, case C, is for still larger initial amplitudes and the results presented are obtained via the boundary integral code as the solution would require too many modes for efficient application of the spectral method. Fig. 8, for $\epsilon\beta = -0.50$, is a result for conditions well within the region of instability $|\epsilon\beta| \leqslant 1.22$. Of particular significance is the rapid growth of the higher modes in this case: the P_4 amplitude exceeds 0.2 by $\omega_0 t/2\pi = 5$ and the

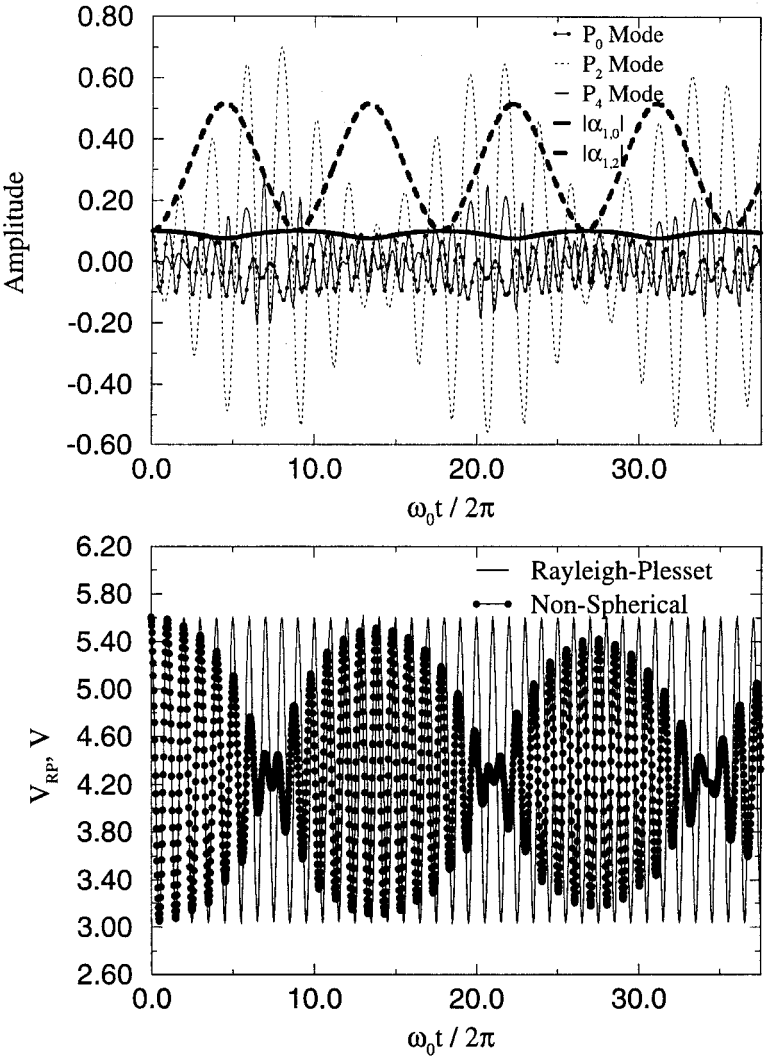

Fig. 9. Amplitudes of the P_0, P_2 and P_4 modes (top) and the volume response V compared with the Rayleigh–Plesset theory V_{RP} (bottom) for Case C (Table 1) with $\epsilon\beta = -1.00$.

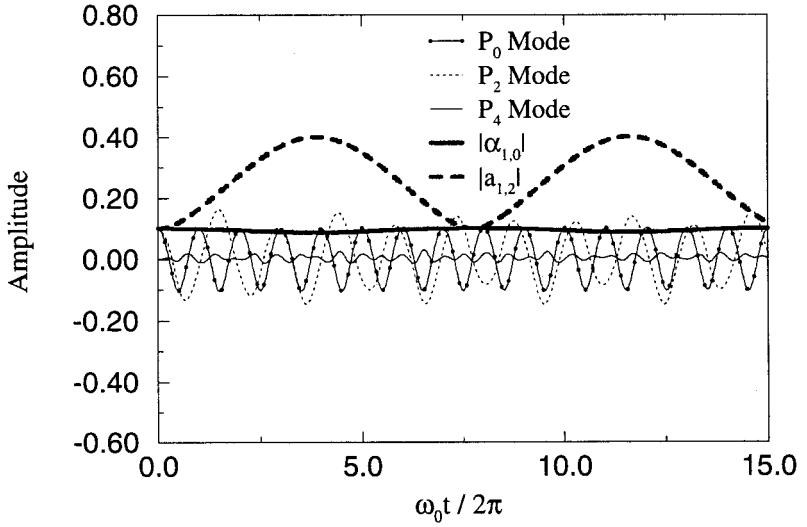

Fig. 10. Amplitudes of the P_0, P_2 and P_4 modes for Case C (Table 1) with $\epsilon\beta = -1.20$.

modes above P_4 rapidly gain amplitude as well, in spite of the fact that it is the P_2 mode that is being directly excited via resonant interaction with the radial oscillations. The actual *volume* of the bubble, including changes in the bubble volume due to changes of shape, is also compared with predictions from the Rayleigh–Plesset theory in Fig. 8. Clearly, the Rayleigh–Plesset theory over-predicts the amplitude of volume oscillations and fails to capture the amplitude modulation that occurs as energy is exchanged between the radial and shape modes. Furthermore, the difference between the finite amplitude, non-spherical bubble simulation and the Rayleigh–Plesset prediction is significant within the first few periods. A close look at the amplitude of the P_0 mode and the bubble volume in Fig. 8 reveals a small, but steady decrease in the maximum amplitude after each exchange with the P_2 mode as the amount of energy available to be returned from the P_2 mode is decreased through interaction with higher modes.

Fig. 9 shows the result for the further detuned case of $\epsilon\beta = -1.00$. As predicted by the small amplitude theory, the period of the amplitude modulation has increased compared to the $\epsilon\beta = -0.50$ case. However, in contrast to the predictions of the small amplitude theory, the *minimum* amplitude of the radial oscillations has decreased. This is a result of more energy being transferred to higher modes during the time that shape mode amplitudes are large; the longer period of the slow modulation of the amplitudes allows more time for energy transfer via mode coupling to occur. The volume response of the bubble still differs significantly from the Rayleigh–Plesset prediction. However, when the level of detuning is slightly increased to $\epsilon\beta = -1.20$ the bubble response dramatically changes to a stable volume oscillation as shown in Fig. 10. It is surprising that this transition is well predicted by the small amplitude theory value of $|\epsilon\beta|_{cr} = 1.22$ even though the amplitudes of the radial and shape oscillations are finite and the unstable oscillations involve many higher order shape modes and the generally poor agreement between the small deformation results and the numerical results for this case.

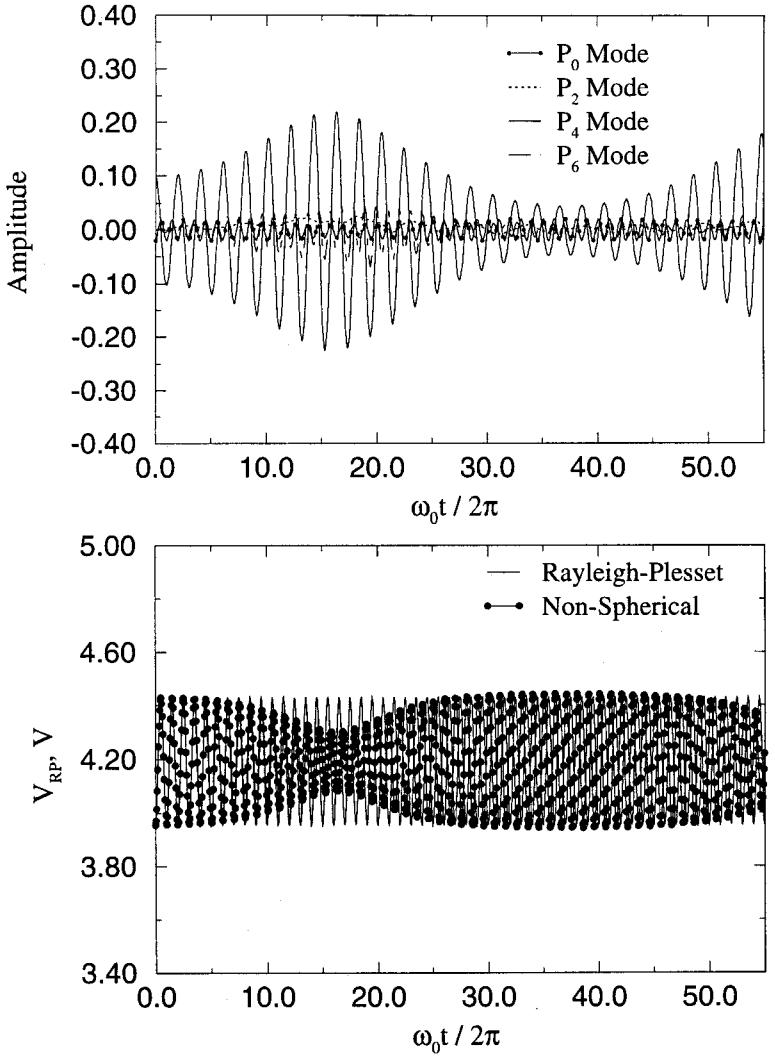

Fig. 11. Amplitudes of the P_0, P_2, P_4 and P_6 modes (top) and the volume response V compared with the Rayleigh–Plesset theory V_{RP} (bottom) for Case D (Table 2) with $\epsilon\beta = -1.00$.

Even though the 2:1 resonance results presented so far have all been for interaction with the $n=2$ shape mode, interactions between radial oscillations and P_n mode shape oscillations are expected for all even values of n. However, as the mode number increases, the numerical solution of the problem requires smaller time-steps as the frequency of oscillation is increased and, eventually, also finer spatial resolution to capture the small length-scale, high mode oscillations. Figs. 11 and 12 show the response of a bubble under 2:1 resonance conditions for $n=4$. The initial disturbances and the predicted critical value of $|\epsilon\beta|_{cr}$ appear in Table 2. In Fig. 11 the interaction between the radial and P_4 shape mode exhibits the continuous exchange of energy seen in the $n=2$ examples. The excitation of higher modes is also evident with the

Table 2
The initial radial and shape disturbances and the predicted critical value of the detuning parameter

Case	$\epsilon\alpha_{1,0}$	$\epsilon\alpha_{1,4}$	$\lvert\epsilon\beta\rvert_{cr}$
D	-0.020	0.100	0.977

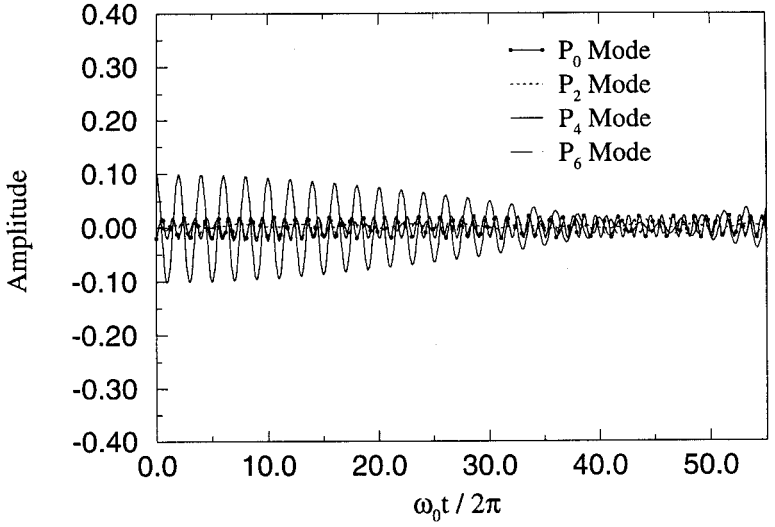

Fig. 12. Amplitudes of the P_0, P_2 and P_4 modes for Case D (Table 2) with $\epsilon\beta = -1.20$.

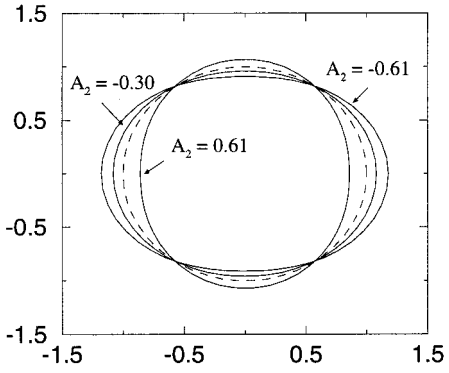

Fig. 13. The steady-state shapes for bubbles described in Table 3 with non-spherical mean shapes. There is rotational symmetry about the x-axis. There are two prolate bubbles, $A_2 = -0.30$, -0.61, and an oblate bubble, $A_2 = 0.61$, shown with a sphere (the dashed line) for reference.

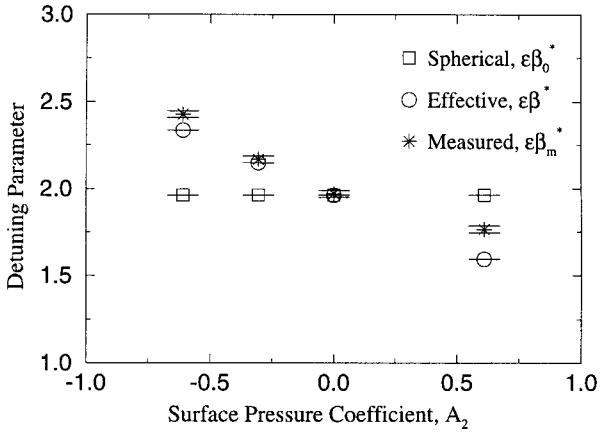

Fig. 14. The theoretical estimates of the detuning, $\epsilon\beta^*$, compared to the result from simulations, $\epsilon\beta_m^*$, for the mean shapes in Table 3 and shown in Fig. 13 with $\epsilon\beta_0^* = 1.96$.

appearance of P_6 shape mode oscillations as the P_4 amplitude grows. A weak P_2 deformation also appears when the P_4 amplitude is large. The origin of the P_2 deformation and oscillation is not explained by the small amplitude theory. However, the departure from Rayleigh–Plesset theory, Fig. 11, and the dramatic transition from unstable to stable radial oscillations near the critical value predicted by small amplitude theory are evident for this case with $\omega_0 \approx 2\omega_4$. Fig. 12 shows an exchange of energy between the P_4 shape mode and radial oscillations, but there is no significant change in the amplitude of radial oscillations.

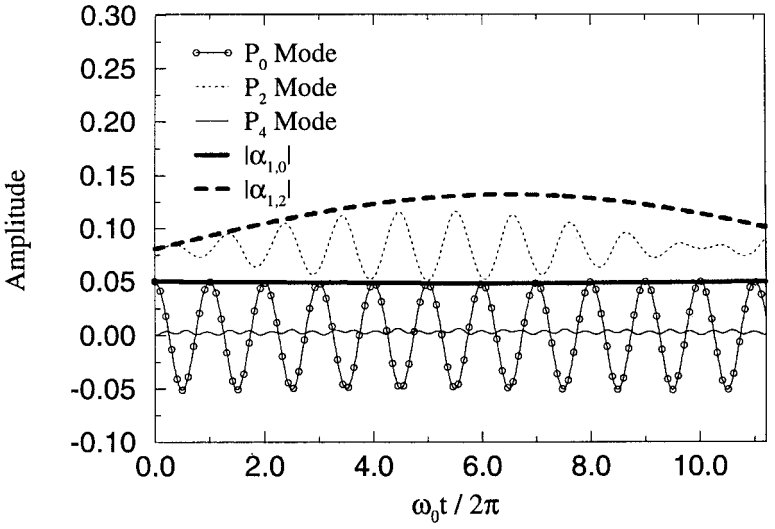

Fig. 15. Amplitudes of the P_0, P_2 and P_4 modes for Case E (Table 3) with $\epsilon\beta^* = 0.25$.

Table 3
The equilibrium values of $\epsilon\alpha_{1,0}$, $\epsilon\alpha_{1,2}$ and the corresponding values of A_0 and A_2

Case	$\epsilon\alpha_{1,0}^{SS}$	$\epsilon\alpha_{1,2}^{SS}$	A_0	A_2
A–D	0.00	0.00	0.00	0.00
E	0.00	0.08	$O(10^{-3})$	−0.30
F	0.00	0.18	$O(10^{-3})$	−0.61
G	0.00	−0.14	$O(10^{-3})$	0.61

4.2. Free oscillations of a bubble with a non-spherical mean shape

For a non-spherical bubble in a quiescent fluid 1:1 resonance between the volume and P_n shape mode oscillations becomes possible when the mean deformation of the bubble involves the P_n mode and $\omega_0 \approx \omega_n$. In the present study, the steady-state shape of the bubble is made non-spherical by a non-uniform pressure distribution imposed on the interface that is described by the pressure coefficients, A_0 and A_n outlined in Section 2. According to the small amplitude theory for 1:1 resonance, the behavior of the bubble does not change abruptly at a critical level of detuning. Instead, the interactions between the radial and shape modes decrease monotonically as the separation of their natural frequencies grows. In these cases, it is important to differentiate between the detuning parameter $\epsilon\beta_0^*$ based upon the natural frequencies for a *spherical* bubble given in Eq. (3) and the *effective* detuning parameter $\epsilon\beta^*$ which accounts for the small amplitude predictions of changes in frequency due to the non-spherical mean shape, as given in Eq. (11). The steady-state amplitudes for the P_0 and P_2 modes and the non-uniform pressure coefficients, A_0 and A_2, for the cases studied are listed in Table 3. The corresponding steady-state shapes are shown in Fig. 13.

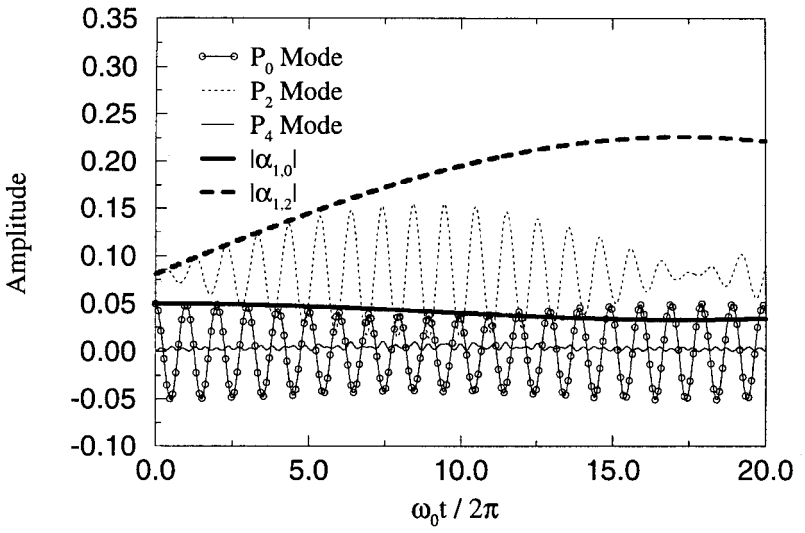

Fig. 16. Amplitudes of the P_0, P_2 and P_4 modes for Case E (Table 3) with $\epsilon\beta^* = 0.05$.

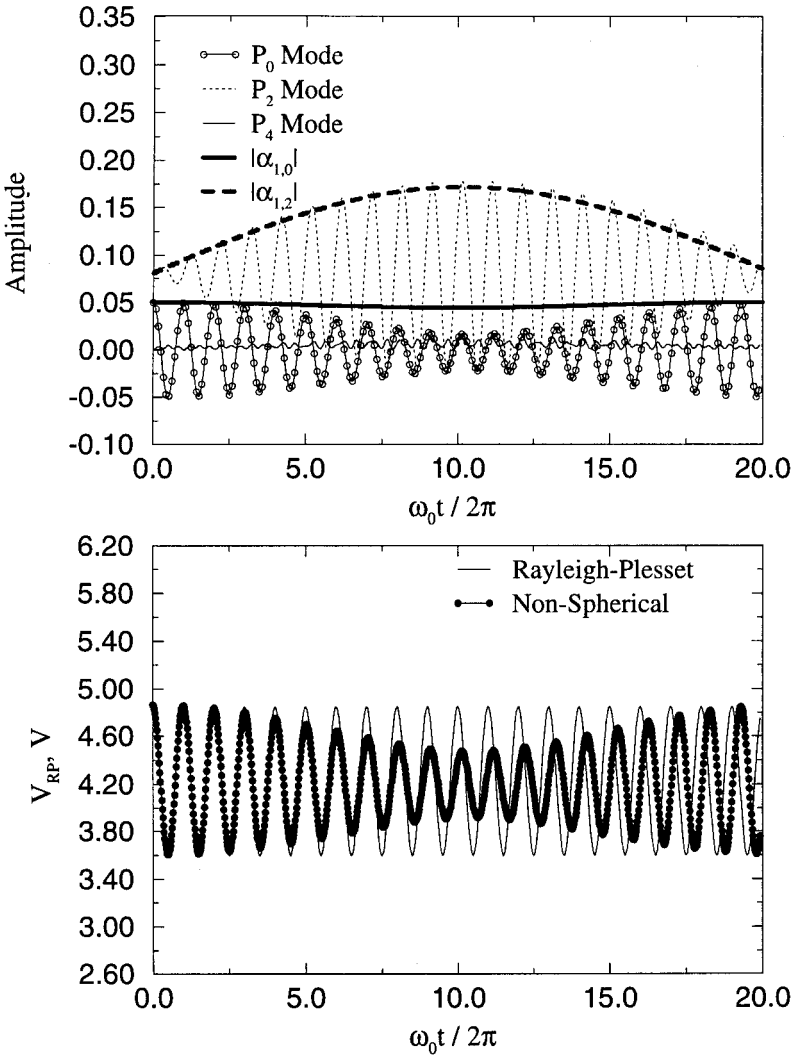

Fig. 17. Amplitudes of the P_0, P_2 and P_4 modes (top) and the volume response V compared with the Rayleigh–Plesset theory V_{RP} (bottom) for Case E (Table 3) with $\epsilon\beta^* = -0.15$.

The qualitative effect of mean deformation on the detuning parameter can be seen in Figure 14. In this figure, the *effective* detuning parameter predicted by the small amplitude theory, $\epsilon\beta^*$, is compared to the amount of detuning measured from numerical stimulations which we denote as $\epsilon\beta_m^*$, for a case where the value for a spherical bubble would be $\epsilon\beta_0^* = 1.96$. The first thing to notice is that the three measures of the detuning are equal *without* a mean deformation. The estimate of the effective detuning parameter from the small amplitude theory varies linearly with the pressure coefficients, A_0 and A_2, as can be seen from Eq. (5). The increase in both the effective and numerically predicted detuning parameters (i.e. the differences in $\omega_0 - \omega_2$) for $A_2 < 0$ is a consequence of the *decrease* in the natural frequency of the shape

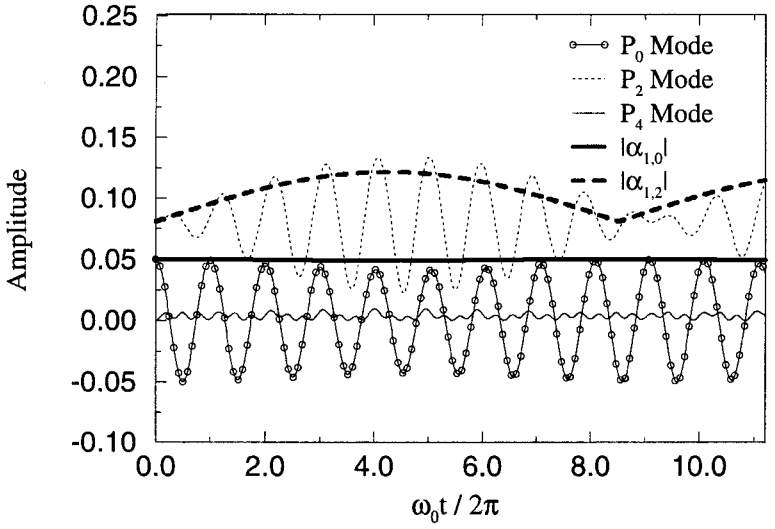

Fig. 18. Amplitudes of the P_0, P_2 and P_4 modes for Case E (Table 3) with $\epsilon\beta^* = -0.35$.

mode for bubbles with a mean prolate shape. Likewise, the decrease in the effective and numerically predicted detuning parameters for $A_2 > 0$ reflects the increase in the natural frequency for shape modes with a mean oblate shape. The simulation results presented below will be identified by the value of the *effective* detuning parameter from the small amplitude theory, $\epsilon\beta^*$, since it can be determined a priori. We note, however, that the exact condition for maximum resonance will not generally be $\epsilon\beta^* = 0$, as can be seen from Fig. 14.

The first series of results are for case E in Table 3 where the mean shape is a *prolate* spheriod with the steady-state shape given by $\epsilon\alpha_{1,0}^{SS} = 0.0$ and $\epsilon\alpha_{1,2}^{SS} = 0.08$. The bubble interface is set in motion by an initial perturbation of the bubble radius. It will be noted from Fig. 14 that the *actual* detuning generally *exceeds* that predicted by small amplitude theory, meaning that the decrease in frequency of the shape mode is smaller than what is predicted by the small deformation theory. Hence, for finite mean prolate deformation, we may anticipate that the *effective* detuning parameter, $\epsilon\beta^*$, will need to be negative to achieve maximum resonance. For case E, calculations were carried out for values of the effective detuning parameter over the range $-0.95 < \epsilon\beta^* < 0.85$, and selected results appear in Figs. 15–18. In Fig. 15, the response for $\epsilon\beta^* = 0.25$ illustrates a relatively weak interaction where the shape mode is clearly active, but the amplitude of oscillation is such that the radial mode appears to maintain a constant amplitude. In this case, the small deformation theory does a modestly good job of predicting the bubble behavior, even though the amplitudes of the deformation are not small. As the detuning parameter is decreased to $\epsilon\beta^* = 0.05$, Fig. 16 shows an increase in the strength of the exchange of energy between the P_0 and P_2 modes. However, Fig. 16 still shows only a modest level of interaction between P_0 and P_2, and almost no higher order modes. In this case, the predicted trajectories from the small amplitude theory are further from the numerical results. The small amplitude theory *overestimates* the strength of the P_0–P_2 interaction. In fact, we shall see that the interactions in this case, according the small amplitude theory, should be the

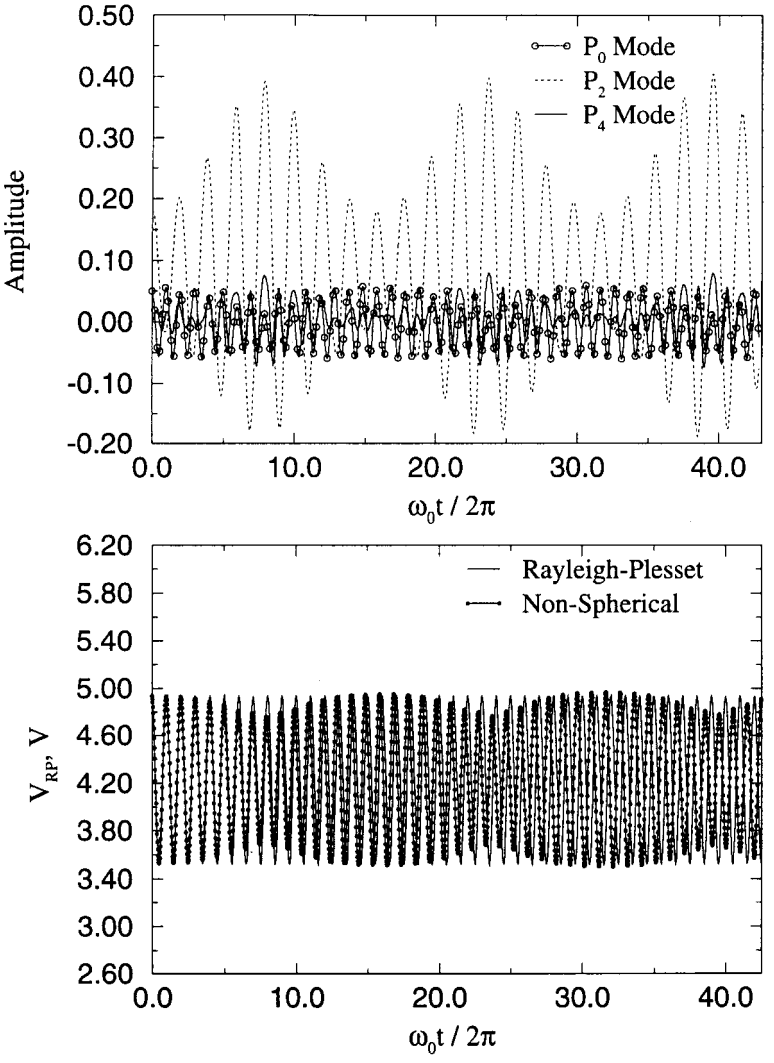

Fig. 19. Amplitudes of the P_0, P_2 and P_4 modes (top) and the volume response V compared with the Rayleigh–Plesset theory V_{RP} (bottom) for Case E (Table 3) with $\epsilon\beta = 0.17$.

strongest of all the cases from 'case E' that we consider. For these simulations, it may be noted in Figs. 15 and 16 that the phase difference between the P_0 and P_2 modes is $\phi = \pi$ when the shape oscillations achieve their maximum amplitude. According to the small amplitude theory, the phase angle at the point when the shape mode has its largest amplitude, should change from π to 0, as we go from the actual $\epsilon\beta > 0$ to $\epsilon\beta < 0$, with the transition point corresponding to exact resonance. The case $\epsilon\beta^* = -0.15$ is shown in Fig. 17. We see that there is stronger energy exchange between modes, with a significant decrease in the amplitude of volume change relative to Rayleigh–Plesset predictions. Now, however, the modes are *in phase* (i.e. $\phi = 0$) as the shape mode oscillations reach their maximum amplitude, indicating that the frequency of

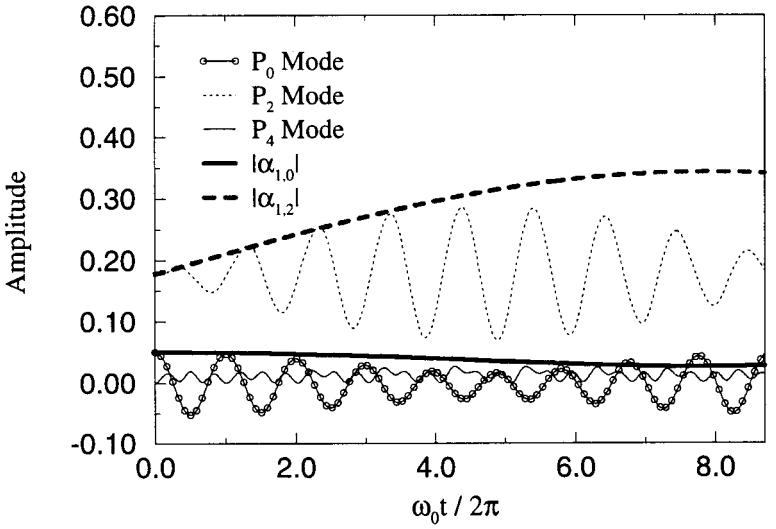

Fig. 20. Amplitudes of the P_0, P_2 and P_4 modes for Case F (Table 3) with $\epsilon\beta^* = -0.16$.

the volume mode is now less than that of the shape mode and we have passed the *actual* resonance condition. The transition thus occurs between $\epsilon\beta^* = 0.05$ and -0.15 in qualitative agreement with the prediction of the small amplitude theory and as expected in light of the agreement between the actual and effective detuning parameters for this case, $A_2 = -0.30$, shown in Fig. 14. Perhaps the most important feature of Fig. 17 is the significant decrease in radial mode oscillations. When compared to the Rayleigh–Plesset result for a bubble of the same volume and initial disturbance, it is clear that the Rayleigh–Plesset theory overestimates the amplitude of the volume oscillation. It is somewhat of a surprise to find such a large effect for this weakly deformed case. The small amplitude theory, in this case, does a reasonable job of predicting the amplitude modulation of the P_2 mode, but it does relatively poorly in predicting the decrease of the radial mode oscillation. This is because a significant portion of the energy transferred to shape oscillations actually goes to higher-order modes that do not appear in the small amplitude theory. As the effective detuning parameter is further decreased, it can be seen in Fig. 18, $\epsilon\beta^* = -0.35$, that the amount of energy exchanged between modes again decreases as we move away from the resonance condition; that there is only weak excitation of shape modes other than P_2; and the small amplitude theory is in reasonable accord with the full numerical results.

It is important to emphasize that the 2:1 resonant interaction also occurs for bubbles with a mean deformation of shape. The main difference, relative to the results of the previous section for an undeformed bubble, is that we must use the effective detuning parameter from Eq. (4) to estimate proximity to resonance, rather than $\epsilon\beta_0 = 0$. To illustrate this point, Fig. 19 shows a typical result in the neighborhood of the 2:1 resonance condition. The volume response of the non-spherical bubble is clearly over-predicted by the Rayleigh–Plesset theory. In this example the effective detuning parameter for 2:1 resonance has a value of $\epsilon\beta = 0.17$ which is within the unstable region, $|\epsilon\beta| \leqslant 0.45$, predicted by small amplitude theory for case E. For bubbles with a

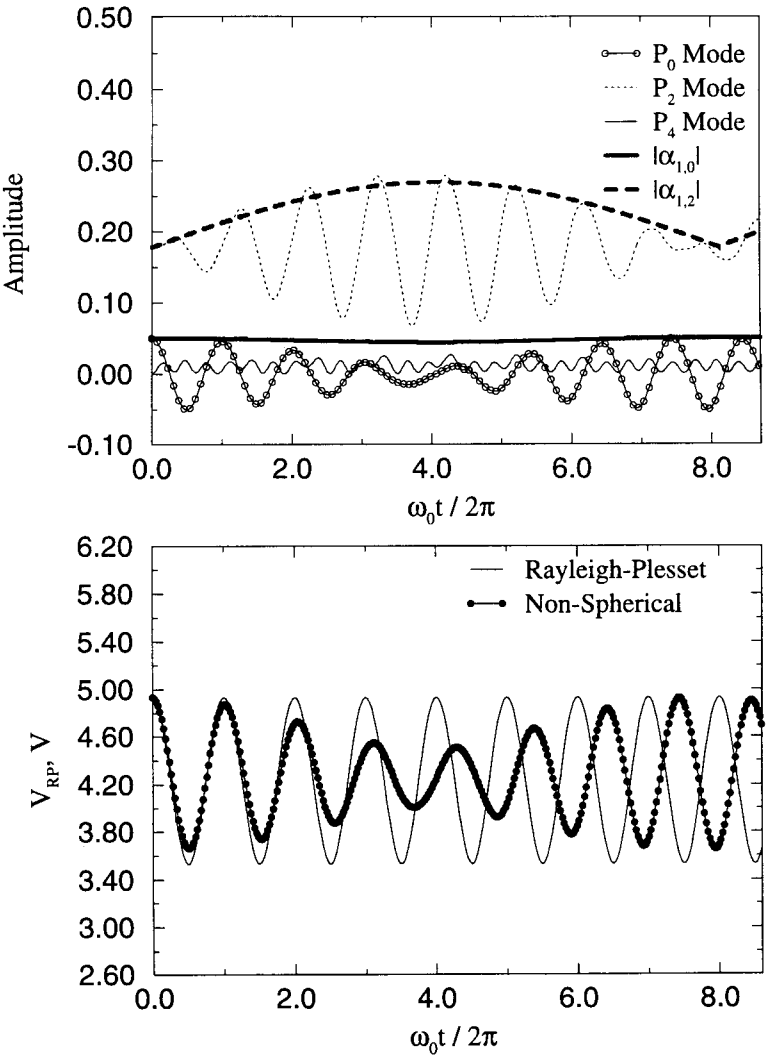

Fig. 21. Amplitudes of the P_0, P_2 and P_4 modes (top) and the volume response V compared with the Rayleigh–Plesset theory V_{RP} (bottom) for Case F (Table 3) with $\epsilon\beta^* = -0.36$.

mean deformation, we therefore have identified two ranges in the natural frequency of radial oscillations where the Rayleigh–Plesset theory does not adequately predict the volume response of an oscillating bubble; the amplitude of the volume response is over-predicted in the neighborhood of both the 1:1 and 2:1 resonance conditions.

In case F of Table 3, the mean deformation has been increased to make the steady-state shape of the bubble more prolate. The interaction between volume and shape oscillations occurs over the frequency range $-0.96 < \epsilon\beta^* < 0.64$ with a noticeable change in the radial response in the range $-0.56 < \epsilon\beta^* < 0.04$ for the same initial radial disturbance of $\epsilon\alpha_{1,0} = 0.05$. The results with the greatest exchange of energy between modes are shown in Figs. 20 and 21

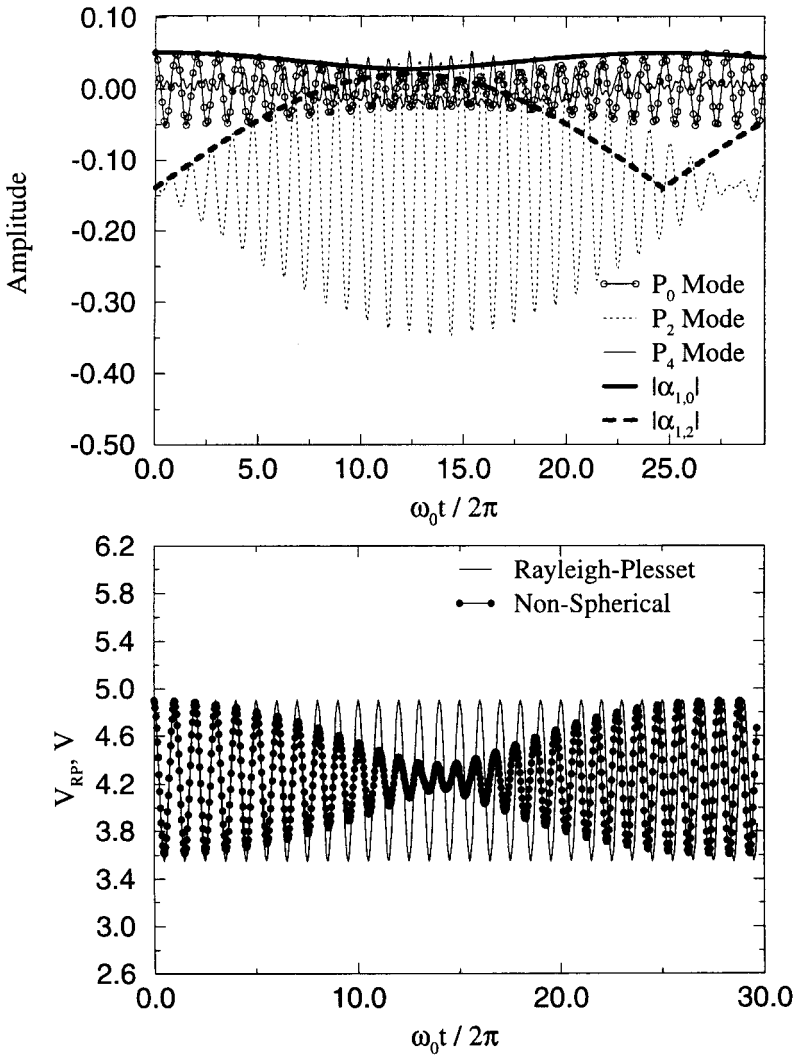

Fig. 22. Amplitudes of the P_0, P_2 and P_4 modes (top) and the volume response V compared with the Rayleigh–Plesset theory V_{RP} (bottom) for Case G (Table 3) with $\epsilon\beta^* = -0.11$.

where the values of the effective detuning parameter are $\epsilon\beta^* = -0.16$ and -0.36, respectively. By looking at the relative phase when the shape oscillations achieve their maximum amplitude we again conclude that these results lie on opposite sides of the actual exact resonant condition. The actual resonant condition does not occur at $\epsilon\beta^* = 0.00$ due to the growing disparity between the actual and effective detuning parameters as the mean deformation increases as seen in Fig. 14. It is again important to note the pronounced decrease in the amplitude of the radial mode oscillations. Indeed, when the volume oscillations for $\epsilon\beta^* = -0.36$ are compared to Rayleigh–Plesset predictions in Fig. 21, a large difference in the amplitude of the bubble response is seen in the first few cycles of the volume oscillation.

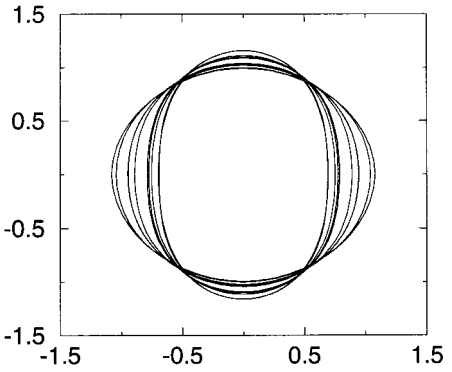

Fig. 23. The evolution of the bubble shapes and the P_2 mode grows for Case G (Table 3) with $\epsilon\beta^* = -0.11$, $\omega_0 t/2\pi = 13 \rightarrow 14$.

The final results we present are for a bubble with a steady-state *oblate* shape corresponding to $\epsilon\alpha_{1,2}^{SS} = -0.14$, case G in Table 3. The oblate spheriod bubble is compressed along the axis of rotational symmetry and in an extreme example would resemble a coin. As for case F, we present results in the vicinity of the exact resonant condition. In Fig. 22, the result for $\epsilon\beta^* = -0.11$ exhibits a *large* growth in the P_2 mode at the expense of radial oscillations. As in the 2:1 resonance case, shape modes of higher order are excited when sufficient energy has been transferred to the shape mode that is directly coupled to the radial oscillations via a resonant interaction. The effect on the volume oscillation of the bubble is shown in Fig. 22 which again demonstrates that the Rayleigh–Plesset equation over-predicts the amplitude of volume oscillations for a bubble that is not restricted to a purely spherical shape. The bubble shapes in

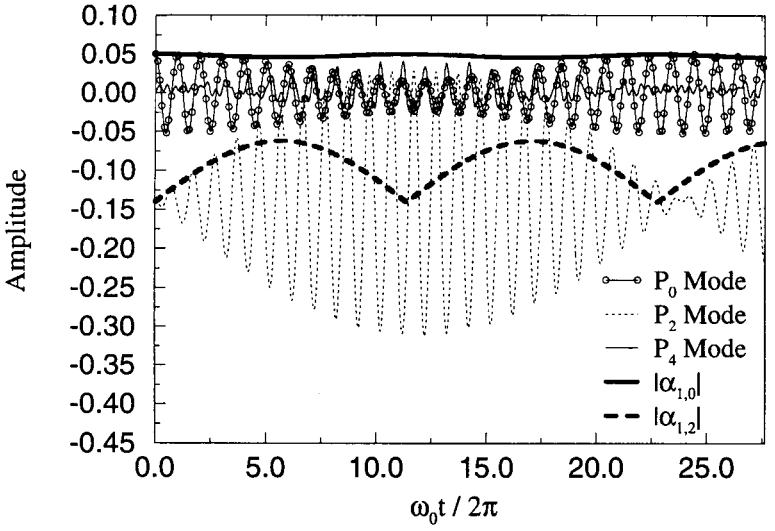

Fig. 24. Amplitudes of the P_0, P_2 and P_4 modes for Case G (Table 3) with $\epsilon\beta^* = -0.21$.

Fig. 23 for $13 < \omega_0 t/2\pi < 14$ reveal how the bubble shape evolves over a period of the radial oscillation. In Fig. 24 where the detuning is $\epsilon\beta^* = -0.21$, the radial and shape oscillations are now out of phase when the shape mode has its largest amplitude in contrast to Fig. 22 where the modes are in phase as the shape mode has its maximum amplitude. This tells us that these two simulations have values of the detuning which bracket the actual resonance condition.

4.3. Bubble breakup

In two phase gas–liquid systems the rates of heat and/or mass transfer are strongly influenced by the interfacial area between the phases. As a result, in gas–liquid mass or heat transfer systems, the bubble size distribution is extremely important. The bubble size distribution is determined by a balance between the rate of bubble breakup and the rate of bubble coallescence. In our study of the dynamics of non-spherical bubbles we have observed two mechanisms of bubble breakup, neither of which requires the large gradients of pressure or velocity that are generally associated with bubble breakup. Instead, these mechanisms require only a large initial perturbation of the bubble volume, that eventually leads to large oscillations of shape via parametric instability or resonant coupling between volume and shape modes. In this section, we present results showing the two mechanisms of bubble breakup that we have observed.

Building on the results for case C in Section 4.1 the initial radial disturbance was increased for a bubble with $\epsilon\beta_0 = -1.00$ with a fixed initial P_2 perturbation of $\epsilon\alpha_{1,2} = 0.10$. The sequence of bubble shapes immediately preceding breakup for $\epsilon\alpha_{1,0} = 0.20$ is shown in Fig. 25. The shapes are axisymmetric about the horizontal axis. In this sequence, the earliest shape, approximately one half period before breakup, is the oblate spheroid corresponding to the outline with the smallest horizontal dimension and the largest vertical dimension. As time progresses, a waist is formed in the bubble as the vertical dimension shrinks until finally the bubble pinches off to form two bubbles with oblate initial shapes. It is noteworthy that the bubble shapes become more complex as the bubble collapses. This appears to be a consequence of the growth of surface waves as the area of the bubble decreases. A corresponding decrease in the complexity of the bubble shape was observed in the expansion phase of the bubble

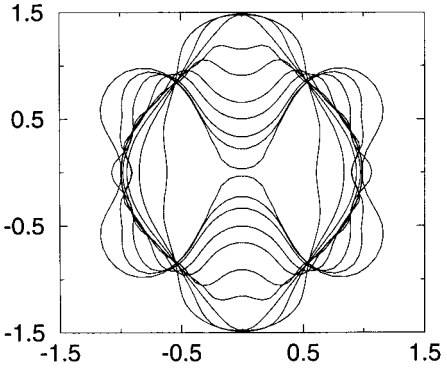

Fig. 25. The evolution of the bubble shapes during the final collapse before breakup.

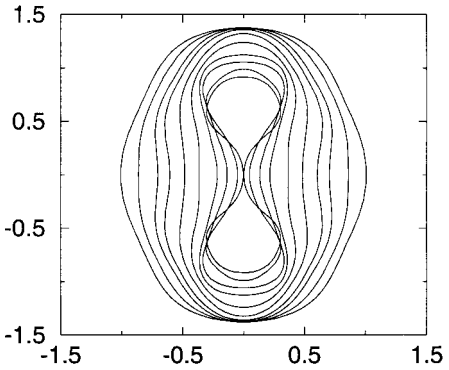

Fig. 26. The evolution of the bubble shapes during the final collapse before breakup via the formation of a toroidal bubble.

which precedes the series of bubble shapes in Fig. 25. It should be noted that bubble breakup was also observed to occur by the formation of a toroidal bubble where the opposite surfaces of the bubble approach along the horizontal axis. This breakup mechanism is illustrated below with an example describing the breakup of a bubble in the presence of a nonuniform pressure field.

Consider now a bubble with the same mean shape as those in case G of Section 4.2 with $\epsilon\beta^* = -0.11$ and an initial radial displacement of $\epsilon\alpha_{1,0} = 0.40$ driving the oscillations. Again the outlines of the bubble shapes just preceding breakup are presented in Fig. 26. In contrast to the earlier bubble breakup result, the collapse of the bubble is more pronounced along the horizontal axis and the collapse results in the formation of a toroidal bubble. We do not endeavor to follow the bubble evolution beyond the contact of the opposing surfaces, but it is reasonable to assume that the toroidal bubble further breaks into several bubbles via a capillary wave-like instability. The final result of the breakup mechanism would then be a ring of smaller bubbles. This mechanism for bubble breakup has also been suggested by Longuet-Higgins (1990). An insufficient number of simulations have been done to determine which, if either, method of bubble breakup occurs most frequently.

5. Summary of results

5.1. Bubbles with a spherical mean shape

- 2:1 resonant coupling between purely radial and a single shape mode oscillation results in a continuous exchange of energy between modes. The strength of the interaction—the amount of energy exchanged—depends upon the proximity to the resonance condition in agreement with small deformation theory, cf. Figs. 2 and 3.
- Finite amplitude deformations lead to excitation of higher order shape modes and energy transfer mechanisms beyond the scope of small deformation theory. The cascade of energy

to into higher order modes results in a slow decrease in the amplitude of volume oscillations. However, theory is able to provide a conservative estimate of the frequency range over which the purely radial oscillations are 'unstable' and lead to large oscillations of bubble shape, cf. Figs. 4–7, 8–10, and 11–12.
- The volume response of bubbles near resonant conditions is markedly different than that predicted by Rayleigh–Plesset theory which over-predicts the amplitude of volume oscillations when energy has been transfered to shape mode oscillations, cf. Figs. 8 and 9.
- The resonant interaction is not *necessarily* between purely radial and P_2 mode oscillations. Fig. 11 shows the impact on the volume response for the interaction between radial and P_4 mode oscillations.

5.2. Bubbles with a non-spherical mean shape

- In the presence of a mean deformation, the volume response of a bubble in the neighborhood of 1:1 resonant conditions shows significant deviation from Rayleigh–Plesset theory within the first few cycles of oscillation, cf. Figs. 17, 21 and 22.
- The small deformation theory provides a reasonable estimate of the amount of energy exchanged between modes as the proximity to resonant conditions varies, but does not consistently predict the details of the interaction between modes. Most notably the theory often fails to capture the period of the slow variation in the oscillation amplitudes.
- The 2:1 resonant interaction can still occur for bubble with a mean non-spherical shape, cf. Fig. 19.
- The magnitude of the mean deformation directly impacts the interaction between modes, as seen by comparing cases E and F.
- The nature of the bubble response remains unchanged regardless of whether the mean deformation results in a prolate or oblate spheriod bubble, cf. cases F and G.

5.3. Bubble breakup

- Transfer of energy from finite amplitude radial oscillations to shape oscillations via resonant and/or finite amplitude interactions can lead to bubble breakup.
- Two methods of bubble breakup have been observed that result in the bubble collapsing to form either two smaller oblate spheriod bubbles or a toroidal bubble which is likely to further break to form several smaller bubbles, cf. Figs. 25 and 26.

6. Conclusions

The numerical results presented in the previous sections illustrate the importance of both volume and shape oscillations on the dynamics of oscillating bubbles and suggest that both

must be considered when trying to predict the response of a bubble to finite amplitude disturbances. The small amplitude analysis from earlier studies serves as a roadmap which aids in the interpretation of the results at finite amplitude. In addition, the small amplitude theory provides *conservative* estimates for the limit of stability of spherical oscillations over the entire range of conditions considered in the investigation of the 2:1 resonant interactions for bubbles with a spherical equilibrium shape. Surprisingly, this is even true for the large amplitude example, case C, when the shape oscillations of the bubble involve many higher order modes that effect the bubble dynamics.

Oscillations of shape are important over a broad range of frequencies when the bubble oscillations are of finite amplitude. The decrease in the amplitude of radial oscillations as shape oscillations are excited provides a possible explanation for the over-prediction of sound generated by an oscillating spherical bubble given by the Rayleigh–Plesset equation. The presence of even a slightly non-uniform pressure leading to a deformed mean shape leads to significant deviation from the Rayleigh–Plesset prediction for the volume response of a bubble. Furthermore, numerical results for bubbles with a mean deformation identify two frequency ranges, corresponding to 2:1 and 1:1 resonance, where the Rayleigh–Plesset theory is insufficient to describe the volume response of an oscillating bubble.

The excitation of higher order shape modes provides a mechanism for additional decreases in the amplitude of radial oscillations. Even without viscous dissipation the excitation of higher modes reduces the amount of energy available to drive radial oscillations. If the energy transferred to higher modes is removed via dissipation, the bubble response should decrease in amplitude until the interactions between P_0 and P_2 are no longer of sufficient amplitude to excite higher modes.

Bubble breakup is observed to occur via two mechanisms, (1) the bubble fissions into two smaller oblate bubbles, as shown in Fig. 25, or (2) the bubble collapses to form a toroidal bubble, as in Fig. 26, which is assumed to further break into several small bubbles. If the smaller bubbles formed through the first mechanism subsequently break-up following the second breakup route, a number of smaller bubbles would be formed. In this manner, bubble breakup would lead to the formation of a cloud of smaller bubbles. Testing of this hypothesis would require developing a code suitable for studying the breakup of a toroidal bubble.

Acknowledgements

This research was supported via grants from ONR and NASA. NKM was also supported by a doctoral fellowship from NASA. The authors gratefully acknowledge this support.

References

Brebbia, C.A., 1978. The boundary element method for engineers. Halsted Press.

Feng, Z.C., Leal, L.G., 1993. On energy transfer in resonant bubble oscillations. Physics of Fluids A 5, 826–836.

Feng, Z.C., Leal, L.G., 1994. Bifurcation and chaos in shape and volume oscillations of a periodically driven bubble with two-to-one internal resonance. Journal of Fluid Mechanics 266, 1–32.

Feng, Z.C., Leal, L.G., 1997. Nonlinear bubble dynamics. Annual Review of Fluid Mechanics 29, 201–243.

Ffowcs Williams, J.E., Guo, Y.P., 1991. On resonant nonlinear bubble oscillations. Journal of Fluid Mechanics 224, 507–529.

Fletcher, C.A.J., 1991. In: Computational techniques for fluid dynamics, 1. Springer, Berlin.

Kang, I.S., Leal, L.G., 1987. Numerical solution of axisymmetric, unsteady free-boundary problems at finite Reynolds number. I. Finite-difference scheme and its application to the deformation of a bubble in uniaxial straining flow. Physics of Fluids 30, 1929–1940.

Kang, I.S., Leal, L.G., 1988. Small-amplitude perturbations of shape for a nearly spherical bubble in an inviscid straining flow (steady shapes and oscillatory motion). Journal of Fluid Mechanics 187, 231–266.

Kang, I.S., Leal, L.G., 1989. Numerical solution of axisymmetric, unsteady free-boundary problems at finite Reynolds number. II. Deformation of a bubble in a biaxial straining flow. Physics of Fluids A 1, 644–660.

Kang, I.S., Leal, L.G., 1990. Bubble dynamics in time-periodic straining flows. Journal of Fluid Mechanics 218, 41–69.

Longuet-Higgins, M.S., 1989a. Monopole emission of sound by asymmetric bubble oscillations. Part 1. Normal modes. Journal of Fluid Mechanics 201, 525–541.

Longuet-Higgins, M.S., 1989b. Monopole emission of sound by asymmetric bubble oscillations. Part 2. An initial-value problem. Journal of Fluid Mechanics 201, 543–565.

Longuet-Higgins, M.S., 1990. Bubble noise spectra. Journal of the Acoustical Society of America 87, 652–661.

Longuet-Higgins, M.S., 1992. Nonlinear damping of bubble oscillations by resonant interaction. Journal of the Acoustical Society of America 91, 1414–1420.

Lundgren, T.S., Mansour, N.N., 1988. Oscillations of drops in zero gravity with weak viscous effects. Journal of Fluid Mechanics 194, 479–510.

Marston, P.L., 1980. Shape oscillation and static deformation of drops and bubbles driven by modulated radiation stresses—theory. Journal of the Acoustical Society of America 67, 15–26.

McDougald, N.K. 1997 The dynamics of an oscillating non-spherical bubble. Ph.D. thesis, University of California at Santa Barbara, CA.

Mei, C.C., Zhow, X.C., 1991. Parametric resonance of a spherical bubble. Journal of Fluid Mechanics 229, 29–50.

Miksis, M.J., 1981. A bubble in an axially symmetric shear flow. Physics of Fluids 24, 1229–1231.

Plesset, M.S., Prosperetti, A., 1977. Bubble dynamics and cavitation. Annual Reviews of Fluid Mechanics 9, 145–185.

Prosperetti, A., 1984a Bubble phenomena in sound fields: part one, Ultrasonics 69–77.

Prosperetti, A., 1984b Bubble phenomena in sound fields: part two, Ultrasonics 115–124.

Sevik, M., Park, S.H., 1973. The splitting of drops and bubbles by turbulent fluid flow. Journal of Fluids Engineering—Transactions of the ASME 95, 53–60.

Yang, S.M., Feng, Z.C., Leal, L.G., 1993. Nonlinear effects in the dynamics of shape and volume oscillations for a gas bubble in an external flow. Journal of Fluid Mechanics 247, 417–454.